Journal of Zhejiang University-SCIENCE A (Applied Physics & Engineering) 2022 23(12):998-1012
www.jzus.zju.edu.cn; www.springer.com/journal/11582
E-mail: jzus_a@zju.edu.cn

Research Article

https://doi.org/10.1631/jzus.A2200158

Check for updates

Optimum insulation thickness of external walls by integrating indoor moisture buffering effect: a case study in the hot-summer-cold-winter zone of China

Yan-hao FENG[1], Zi-tao YU[1,2]✉, Jiang LU[3], Xu XU[4]

[1]*Institute of Thermal Science and Power Systems, Zhejiang University, Hangzhou 310027, China*
[2]*State Key Laboratory of Clean Energy Utilization, Zhejiang University, Hangzhou 310027, China*
[3]*School of Civil Engineering and Architecture, Zhejiang University of Science and Technology, Hangzhou 310023, China*
[4]*Institute of Energy Engineering, China Jiliang University, Hangzhou 310018, China*

Abstract: In the high-humidity, hot-summer-cold-winter (HSCW) zone of China, the moisture buffering effect in the envelope is found to be significant in optimum insulation thickness. However, few studies have considered the effects of indoor moisture buffering on the optimum insulation thickness and energy consumption. In this study, we considered the energy load of an exterior wall under moisture transfer from the outdoor to the indoor environment. An optimum insulation thickness was obtained by integrating the P_1–P_2 model. A residential building was selected for the case study to verify the proposed method. Finally, a comparison was made with two other widely used methods, namely the transient heat transfer model (TH) and the coupled heat and moisture transfer model (CHM). The results indicated that the indoor moisture buffering effect on the optimum insulation thickness is 2.54 times greater than the moisture buffering effect in the envelope, and the two moisture buffering effects make opposing contributions to the optimum insulation thickness. Therefore, when TH or CHM was used without considering the indoor moisture buffering effect, the optimum insulation thickness of the southern wall under one air change per hour (1 ACH) and 100% normal heat source may be overestimated by 2.13% to 3. 59%, and the annual energy load on a single wall may be underestimated by 10.10% to 11.44%. The decrease of airtightness and the increase of indoor heat sources may result in a slight reduction of optimum insulation thickness. This study will enable professionals to consider the effects of moisture buffering on the design of insulation thickness.

Key words: Insulation thickness optimization; Coupled heat and moisture transfer; Indoor moisture buffering effect; Exterior wall; Lifecycle cost

1 Introduction

The total energy consumption of buildings takes up to 30% of primary energy usage and a suitable insulation thickness of external walls can save about 30% of the total building energy consumption (Fang et al., 2014; Chen et al., 2020). The optimum insulation thickness is often determined by a techno-economic analysis. There are two groups of methods for that analysis: static methods and dynamic methods (Kaynakli, 2012). Static ones, such as the concept of degree day (Ali Kallioğlu et al., 2021), are classic and easy to use. Dynamic methods, such as analytical solutions based on periodic atmospheric temperatures (Zhang et al., 2022) and numerical solutions under more general meteorological conditions (Dlimi et al., 2019; Wang et al., 2019; Geng et al., 2021), can take into account transient changes in outdoor air temperature. However, the role of moisture in the air is often neglected.

The average relative humidity of air in the hot-summer-cold-winter (HSCW) zone is close to 75%–80%. For residential buildings, the high-humidity environment can cause moisture-related health problems such as mould-growth (Woods and Winkler, 2016). In addition, the material in the exterior wall of a residential building can absorb a large amount of moisture. This adsorbed moisture can produce a significant moisture buffering effect in the envelope, thereby increasing the average heat capacity and thermal conductivity

✉ Zi-tao YU, yuzitao@zju.edu.cn
Yan-hao FENG, https://orcid.org/0000-0001-7287-1532

Received Mar. 26, 2022; Revision accepted July 4, 2022;
Crosschecked Nov. 4, 2022

of its materials. By calculating the heat, air, and moisture transfer (HAM) equations, it was shown that the moisture transfer can have a significant impact on the assessment of building energy consumption (Tariku et al., 2010; Hens, 2015; Xu et al., 2019; Chung et al., 2020). Moon et al. (2014) investigated the effect of moisture migration on the building performance of a residential apartment by WUFI Plus and showed that the energy consumption was 4.4% higher when moisture buffering effects were considered. Chbani Idrissi et al. (2022) performed an HAM simulation of a residential building in the climate of Tangier by using COMSOL Multiphysics and showed that the annual energy consumption was 15.1% greater than that calculated using the heat transfer model. Recently, a study integrating the HAM and the techno-economic analysis using COMSOL Multiphysics was carried out (Liu et al., 2015). It showed that if the moisture buffering effect in the envelope is not considered, the optimal insulation thickness and energy consumption of a typical residential building in the HSCW zone in China could be underestimated by 3.7%–7.8% and 2.8%–8.4%, respectively.

However, the moisture buffering effect is combined with various other factors, such as temperature and humidity distribution in the indoor and outdoor atmosphere, airtightness, and heating, ventilating, and air conditioning (HVAC) systems (Fang et al., 2022). Specifically, the indoor environmental performance of a residential building in the HSCW zone is shown to be the least satisfactory in China (Li et al., 2018), and the indoor moisture buffering effect can cause high indoor energy consumption and indoor humidity fluctuations (Qin et al., 2009; Woloszyn et al., 2009; Qin and Yang, 2016). Therefore, a comprehensive evaluation of the moisture buffer effect not only needs to consider the moisture buffer inside the envelope, but also needs to consider the indoor moisture buffer effect. Recently, based on the cases of the building energy simulation test (BESTEST), experiments by Zhang et al. (2017) on porous bricks have shown that hygroscopic materials can reduce fluctuations in indoor relative humidity, and thereby reduce dehumidification energy consumption by 25%–30%. Ferroukhi et al. (2015) compared the energy consumption of a residential building in La Rochelle by two types of software: TRNSYS and COMSOL Multiphysics. The results showed the consequences of TRNSYS ignoring the inclusion of indoor moisture effects can cause an underestimation of energy consumption by 51%. Therefore, keeping the indoor temperature and relative humidity constant in the insulation thickness optimization may ignore the indoor moisture buffering effect and have a bias in the optimum insulation thickness, especially in some special buildings with high indoor moisture generation, such as gymnasiums and swimming pools.

Based on the integration of the HAM and the indoor environment model (IEM), Zhou et al. (2020) analyzed the influence of the indoor moisture buffering effect on the average indoor temperature of a typical residential building by using COMSOL Multiphysics. The results indicated that the desorption cooling from hygroscopic materials can reduce the temperature by 1.31 K in the summer. Under the coupled analysis of HAM and IEM, the total energy consumption, as well as the optimum insulation thickness, can be different from that found in the original studies done by traditional static or dynamic methods. However, few studies have been done in the field. Furthermore, it is not certain how the moisture buffering effect in the envelope and indoor moisture buffering effect have a quantitative effect on the optimal insulation thickness of the exterior wall. Therefore, it is necessary to further study the optimization of the insulation thickness by integrating the HAM, the control of HVAC systems, as well as the IEM into the optimization of the insulation thickness. Further consideration can eliminate the performance difference between the design stage and the actual use stage brought about by the constant value of simplified indoor temperature and humidity, and thus obtain a more reasonable optimal insulation layer thickness (Martínez-Mariño et al., 2021).

In this study, a method called HAM-IEM was used, and the P_1–P_2 method was used for economic analysis to obtain the optimal insulation thickness. The P_1–P_2 method is an economical calculation method that includes lifecycle costs and investment costs. The proposed optimization method can take into account the indoor moisture buffering effect and the moisture buffering effect in the envelope. The optimum insulation thickness in the high-humidity environment in the HSCW zone can be obtained by the proposed method. A comparison was made of different existing optimization methods in the same building and different climate conditions. In addition, the effects of the magnitude

of heat sources and airtightness on the optimum insulation thickness were studied.

2 Methodology

The flow diagram of the optimization process by the HAM-IEM is shown in Fig. 1. The HAM model (in light blue) and IEM (in orange) were combined and co-calculated to obtain the energy loads Q_c and Q_h. The control of the HVAC system was integrated into the IEM. The combination of HAM and IEM was implemented by the heat and moisture exchange at the inner surface of the exterior wall. Specifically, the heat convection coefficient h_i was determined by

$$h_i = 2.03(T_{iamb} - T_i)^{0.14}, \quad (1)$$

where T_{iamb} and T_i are the temperatures of the indoor environment and interior surface of the wall, respectively. The water vapour transfer coefficient $h_{v,i}$ was demonstrated by the Lewis analogy.

Then, the P_1–P_2 method was chosen for the economic analysis and determination of the optimum insulation thickness. The HAM is described in Section 2.1, the IEM is described in Section 2.2, the combination strategy is described in Section 2.3, and the economic method is described in Section 2.4.

2.1 HAM model

An HAM model was developed to reflect the effect of the outdoor environment and, especially, that of humid air on choosing the optimum insulation thickness. The HAM model consists of a moisture transfer equation, an air transfer equation, and a thermal transfer equation. These equations are derived under the assumptions (Xu et al., 2019): (1) that the materials are homogenous, continuous, and isotropic; (2) that hysteresis and chemical reactions are neglected; (3) that the wall can be simplified as a 1D segment.

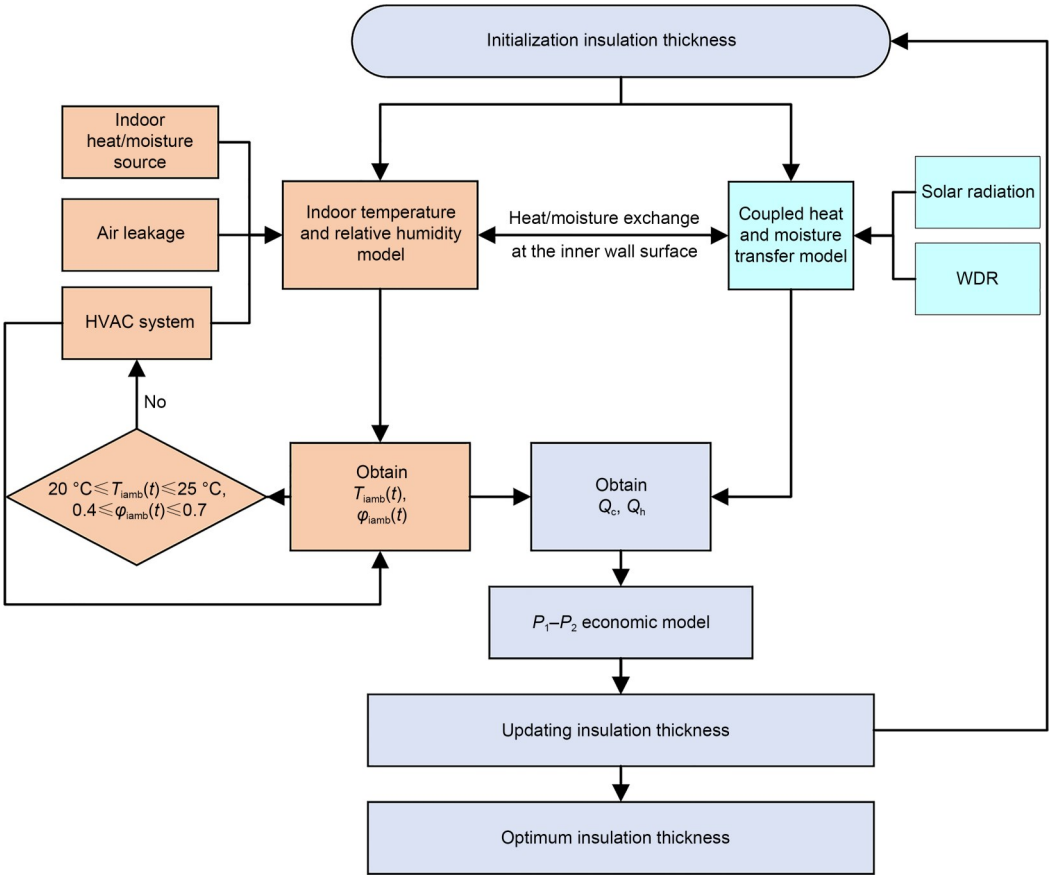

Fig. 1 Flow chart of the optimization integrated with the indoor environment. WDR refers to the wind-driven rain, φ_{iamb} is the relative humidity, t is the time, and Q_c and Q_h are the annual energy loads of a wall in the cooling season and heating season, respectively. References to color refer to the online version of this figure

2.1.1 Governing equations

The governing equations of HAM model that given in Eqs. (2)–(4) contain the moisture transfer equation, air transfer equation, and heat transfer equation, where C_p is the specific heat capacity, $e_\omega=0.622P_v/(P_{atm}-P_v)$ is the absolute air humidity, k_a is the airflow coefficient, L is the latent heat, P is the pressure, R is the gas constant, T is the temperature, and w is the moisture content. $U_a=-k_a(\mathrm{d}P_a/\mathrm{d}x)/\mu_a$ is the air velocity vertical to the wall surface, g is the diffusion, $g_l=-\rho_l R\delta_l\left(\ln\varphi\dfrac{\partial T}{\partial x}+\dfrac{T}{\varphi}\dfrac{\partial\varphi}{\partial x}\right)$ is the liquid water diffusion, $g_v=-\delta_v\left(\varphi\dfrac{\partial P_{bv}}{\partial x}+P_{bv}\dfrac{\partial\varphi}{\partial x}\right)$ is the water vapour diffusion, $g_a=\rho_a\dfrac{k_a}{\mu_a}\dfrac{0.622}{P_{atm}}\left(\varphi P_{bv}\dfrac{\partial P_a}{\partial x}\right)$ is the air diffusion (air convection), ρ is the density, φ is the relative humidity, δ is the permeability, μ_a is the air dynamic viscosity, and subscripts a, atm, bv, c, l, m, and v refer to the air, atmosphere, saturated water vapour, capillary, liquid water, porous matrix, and water vapour, respectively. The effective thermal conductivity λ_{eff} represents the equivalent thermal conductivity of a three-phase porous building material, which is measured by converting heat conduction, convection, and radiation inside the material into an equivalent heat transfer process (Wang et al., 2018). Detailed derivation of the equations is shown in Section S1 of the electronic supplementary materials (ESM).

$$\frac{\partial w}{\partial\varphi}\frac{\partial\varphi}{\partial t}+\frac{\partial w}{\partial T}\frac{\partial T}{\partial t}+\frac{\partial(g_l+g_v+g_a)}{\partial x}=0, \tag{2}$$

$$-\frac{\partial}{\partial x}\left(\delta_a\frac{\partial P_a}{\partial x}\right)=0, \tag{3}$$

$$\left(\rho_m C_{pm}+wC_{pl}\right)\frac{\partial T}{\partial t}+\frac{\partial}{\partial x}\left(-\lambda_{eff}\frac{\partial T}{\partial x}\right)+g_l C_{pl}\frac{\partial T}{\partial x}-L\left(\frac{\partial g_v}{\partial x}+\frac{\partial g_a}{\partial x}\right)+\rho_a\left(C_{pa}+e_\omega C_{pv}\right)\frac{\partial(U_a T)}{\partial x}=0. \tag{4}$$

2.1.2 Boundary conditions

Fig. 2 is a schematic diagram of the boundary conditions in the study. The boundary conditions consist of outdoor and indoor parts.

2.1.2.1 Outdoor boundary conditions

The outdoor boundary conditions, which include the moisture, air, and heat exchanges on the exterior surface of the wall, are expressed as:

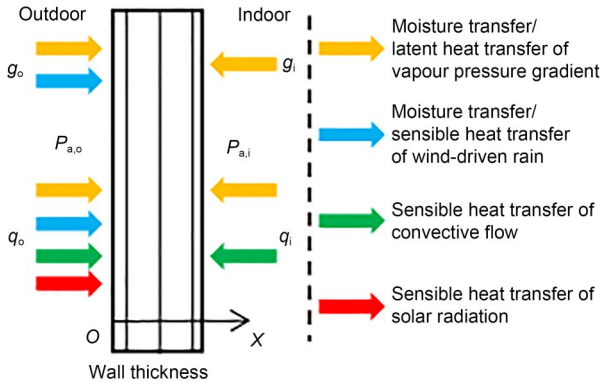

Fig. 2 Schematic diagram of the numerical domain and boundary conditions of HAM. q is the heat flow, and the subscripts o and i refer to the exterior surface and the interior surface of the wall, respectively

$$\begin{aligned}&g_o=h_{v,o}\left(\varphi_{amb}P_{bv,amb}-\varphi_o P_{bv,o}\right)+\kappa I_{WDR},\\&P_{a,o}=P_{amb},\\&q_o=Lh_{v,o}\left(\varphi_{amb}P_{bv,amb}-\varphi_o P_{bv,o}\right)+h_o(T_{amb}-T_o)+\\&\quad\alpha q_{radi}+\kappa I_{WDR}C_{pl}(T_{amb}-T_o),\end{aligned} \tag{5}$$

where h and h_v are the heat convection coefficient and water vapour transfer coefficient, respectively; α=0.6 is the solar absorptivity; q_{radi} is the received solar radiation on the wall; the subscript amb refers to the outside environment. In this study, h_o=23.26 W/(m^2·K), $h_{v,o}=1.79\times10^{-7}$ s/m, L=2500−2.4T kJ/kg, the saturated vapour pressure P_{bv} is a function of the temperature. κ=0.01 is the infiltration coefficient of WDR according to ASHRAE 160; I_{WDR} is the WDR intensity calculated by Trindade et al. (2021):

$$I_{WDR}=k_{avg}\frac{2}{9}C_R C_T O W U_{10}R_h^{8/9}\cos\theta,\quad -90°<\theta<90°, \tag{6}$$

where k_{avg}=0.44, C_R=0.83, C_T=1, O=0.7, and W=0.4 are coefficients; U_{10} is the wind velocity at 10 m; R_h is the rainfall intensity and θ is the included angle between the normal of surface and wind direction. All the meteorological parameters (T_{amb}, φ_{amb}, P_{amb}, q_{radi}, R_h, and the wind direction) were obtained from the National Oceanic and Atmospheric Administration (NOAA) database (NOAA, 2001).

2.1.2.2 Indoor boundary conditions

The indoor boundary conditions, which include the moisture, air, and heat exchanges on the interior surface of the wall, are expressed as:

$$
\begin{aligned}
&g_{\mathrm{i}}=h_{\mathrm{v,i}}\left(\varphi_{\mathrm{iamb}}P_{\mathrm{bv,iamb}}-\varphi_{\mathrm{i}}P_{\mathrm{bv,i}}\right),\\
&P_{\mathrm{a,i}}=P_{\mathrm{amb}}+\Delta P,\\
&q_{\mathrm{i}}=Lh_{\mathrm{v,i}}\left(\varphi_{\mathrm{iamb}}P_{\mathrm{bv,iamb}}-\varphi_{\mathrm{i}}P_{\mathrm{bv,i}}\right)+h_{\mathrm{i}}(T_{\mathrm{iamb}}-T_{\mathrm{i}}),
\end{aligned}\tag{7}
$$

where ΔP is the pressure difference between indoor and outdoor atmosphere; the subscript iamb refers to the indoor environment. It is noted that the indoor temperature T_{iamb} and relative humidity φ_{iamb} remain to be determined in the IEM.

2.1.3 Validation of HAM

The HAM model proposed in this study is validated with heat, air, and moisture standardization (HAMSTAD) benchmarks #4 and #5. The detailed information about HAMSTAD benchmarks #4 and #5 can be referred to elsewhere (Hagentoft et al., 2004). Figures related to the comparisons can be seen in Section S2 of the ESM. The mean absolute errors (MAEs) between the results of the HAM model and the results in the HAMSTAD project #4 are 3.41 kg/m^3 (exterior) and 15.26 kg/m^3 (interior). The MAE between the results of the HAM model and the results in the HAMSTAD project #5 is 3.02 kg/m^3. Therefore, the proposed model has a good agreement with the benchmarks.

2.2 IEM model

To reflect the influence of the indoor environment (e.g., indoor temperature and relative humidity) on the optimization of insulation thickness, an IEM model is presented in this section. The HVAC systems, indoor heat and moisture sources, and air leakage (airtightness) are considered in the IEM. To increase the efficiency of optimization, the IEM in this study is a reduced-order model that neglects the influence of airflow and buoyancy. As shown in Eq. (8), the IEM model can be written in the form of indoor temperature and relative humidity based on the heat and moisture balance equations, where V is the total volume of the room, ω is the humidity ratio, M_{iamb} and Q_{iamb} are indoor moisture source and heat source, respectively, Q_{mH} and Q_{mlH} are respectively the sensible and latent heat caused by moisture sources, and the superscript T refers to source types, in which b, le, me, oc, and r are the exchanges between the indoor air and hygroscopic wall, outside atmosphere (air leakage), HVAC systems, occupants/other types of mechanical systems, and direct radiation through windows, respectively.

$$
\begin{aligned}
&\rho_{\mathrm{a}}V\frac{\partial\omega_{\mathrm{iamb}}}{\partial t}=\\
&\rho_{\mathrm{a}}V\frac{\partial}{\partial t}\left(\frac{0.622\varphi_{\mathrm{iamb}}P_{\mathrm{bv}}}{P_{\mathrm{atm}}-\varphi_{\mathrm{iamb}}P_{\mathrm{bv}}}\right)=\sum_{\mathrm{T}\in\{\mathrm{b,\ le,\ me,\ oc}\}}M_{\mathrm{iamb}}^{\mathrm{T}},\\
&\rho_{\mathrm{a}}V\frac{\partial}{\partial t}\left[C_{\mathrm{pa}}T_{\mathrm{iamb}}+\left(L+C_{\mathrm{pv}}T_{\mathrm{iamb}}\right)\omega_{\mathrm{iamb}}\right]=\\
&\quad\sum_{\mathrm{T}\in\{\mathrm{b,\ le,\ me,\ oc,\ r}\}}Q_{\mathrm{iamb}}^{\mathrm{T}}+\sum_{\mathrm{T}\in\{\mathrm{b,\ le,\ me,\ oc}\}}Q_{\mathrm{mH}}^{\mathrm{T}}+\\
&\quad\sum_{\mathrm{T}\in\{\mathrm{b,\ le,\ me,\ oc}\}}Q_{\mathrm{mlH}}^{\mathrm{T}}.
\end{aligned}\tag{8}
$$

M_{iamb}, Q_{iamb}, Q_{mH}, and Q_{mlH} in Eq. (8) can be further presented as:

$$
\begin{aligned}
&M_{\mathrm{iamb}}^{\mathrm{b}}=Ah_{\mathrm{v,i}}\left(\varphi_{\mathrm{i}}P_{\mathrm{bv,i}}-\varphi_{\mathrm{iamb}}P_{\mathrm{bv,iamb}}\right),\\
&M_{\mathrm{iamb}}^{\mathrm{le}}=\rho_{\mathrm{a}}VA_{\mathrm{CH}}(\omega_{\mathrm{amb}}-\omega_{\mathrm{iamb}}),\\
&M_{\mathrm{iamb}}^{\mathrm{me}}=\mathrm{Vo}_{\mathrm{HVAC}}\rho_{\mathrm{a}}\mathrm{SET}_{\varphi},\\
&Q_{\mathrm{iamb}}^{\mathrm{b}}=Ah_{\mathrm{i}}(T_{\mathrm{i}}-T_{\mathrm{iamb}}),\\
&Q_{\mathrm{iamb}}^{\mathrm{le}}=\rho_{\mathrm{a}}C_{\mathrm{pa}}VA_{\mathrm{CH}}(T_{\mathrm{amb}}-T_{\mathrm{iamb}}),\\
&Q_{\mathrm{iamb}}^{\mathrm{me}}=\mathrm{Vo}_{\mathrm{HVAC}}\rho_{\mathrm{a}}\left(C_{\mathrm{pa}}+\varphi_{\mathrm{iamb}}C_{\mathrm{pv}}\right)\mathrm{SET}_{T},\\
&Q_{\mathrm{mH}}^{\mathrm{T}}=C_{\mathrm{pv}}(T_{\mathrm{s}}^{\mathrm{T}}-T_{\mathrm{iamb}})\,M_{\mathrm{iamb}}^{\mathrm{T}},\\
&Q_{\mathrm{mlH}}^{\mathrm{T}}=LM_{\mathrm{iamb}}^{\mathrm{T}},
\end{aligned}\tag{9}
$$

and

$$
\begin{aligned}
&\mathrm{SET}_{\varphi}=\begin{cases}0, & 0.4\leqslant\varphi_{\mathrm{iamb}}\leqslant 0.7,\\ \varphi_{\mathrm{HVAC}}-\varphi_{\mathrm{iamb}}, & \text{others},\end{cases}\\
&\mathrm{SET}_{T}=\begin{cases}0, & 293.15\ \mathrm{K}\leqslant T_{\mathrm{iamb}}\leqslant 298.15\ \mathrm{K},\\ T_{\mathrm{HVAC}}-T_{\mathrm{iamb}}, & \text{others},\end{cases}
\end{aligned}\tag{10}
$$

where A and A_{CH} are the total wall area and the air change per hour, respectively; $\mathrm{Vo}_{\mathrm{HVAC}}$ is the total air volume of the HVAC system; φ_{HVAC} and T_{HVAC} are the outlet relative humidity and temperature of the HVAC system, respectively; SET_{φ} and SET_{T} are the set-points of relative humidity and temperature according to the design values in ISO 13788 (ISO, 2012), respectively; T_{s} is the temperature of moisture sources and can be determined from Eq. (9); $Q_{\mathrm{iamb}}^{\mathrm{me}}$ is the power of the HVAC system. $Q_{\mathrm{iamb}}^{\mathrm{me}}$ cannot exceed the maximum capacity of the HVAC system $Q_{\mathrm{iamb,\ max}}^{\mathrm{me}}$. $Q_{\mathrm{iamb}}^{\mathrm{oc}}$ and $M_{\mathrm{iamb}}^{\mathrm{oc}}$ can be simply expressed as a periodical function with period of one day according to the schedule.

The opening of doors and windows is impractical in an air-conditioned room, and the heat and moisture sources such as the water reservoir, wet surfaces,

and airflow through the windows are small. Therefore, compared to the indoor model proposed by Tariku et al. (2010), the terms of moisture and heat sources were simplified in the IEM model in this study. Besides, the validation of the IEM model can be found in (Rode et al., 2006; Tariku et al., 2010).

2.3 Calculation strategy

2.3.1 Energy loads of a single wall Q_c and Q_h

The annual energy loads of a wall in the cooling season Q_c and in heating season Q_h were calculated by:

$$\begin{cases} Q_c = \sum^{Nch} q_c = \sum^{Nch} h_i (T_i - T_{iamb})^+, \\ Q_h = \sum^{Nhh} q_h = \sum^{Nhh} h_i (T_{iamb} - T_i)^+, \end{cases} \tag{11}$$

where q_c and q_h are the instantaneous transmission loads of cooling and heating, respectively; Nch and Nhh are the total hours in the cooling season and heating season, respectively; the superscript + represents that only the positive values are added. T_i and T_{iamb} are time-dependent variables. The cooling season is from June 15 to Aug. 31, and the heating season is from Dec. 1 to Feb. 28 (MOHURD, 2010).

2.3.2 Calculation settings

The HAM-IEM was calculated by the commercial software COMSOL Multiphysics. The transient module and the incident module were used in the numerical calculation and control of the HVAC system, respectively. Since the dimension of the IEM model is zero-dimension, the boundary ordinary differential equation module was used to calculate the lumped indoor temperature and relative humidity. The time step for calculation was set as 10 min.

It should be noted that although the indoor environment is controlled by HVAC systems, the fluctuations and deviations of indoor temperature/relative humidity to the set points can still exist in reality. The HVAC system was set as activated during the cooling or heating season and closed during the non-cooling-or-heating seasons. The humidification/dehumidification system in HVAC was set as open when the relative humidity was beyond the range of 0.4–0.7, and the delay time for the switch on/off was set as 30 min. The control system of HVAC was implemented within the incident module of COMSOL Multiphysics, and the tolerance of the incident is set as 0.001. In the incident module, the implicit event interface is used to control the switch on/off, and the indicator state interface is used to define the set-points in Eq. (10).

2.4 P_1–P_2 method

The P_1–P_2 method was used for the economic analysis (Duffie and Beckman, 1991). The ratio of life cycle energy cost (P_1), the ratio of life cycle expenditure (P_2), the total lifecycle cost which contains operation costs and investment costs (LCT), and the annual energy saving per unit area by the insulation material (AES) can be solved by:

$$P_1 = \mathrm{PWF}(\mathrm{Ne},\ i,\ d) = \begin{cases} \dfrac{1}{d-i}\left[1 - \left(\dfrac{1+i}{1+d}\right)^{\mathrm{Ne}}\right], & i \neq d, \\ \dfrac{\mathrm{Ne}}{1+i}, & i = d, \end{cases} \tag{12}$$

$$P_2 = D + (1-D)\frac{\mathrm{PWF}(N_{\min},\ 0,\ d)}{\mathrm{PWF}(N_L,\ 0,\ m)} + m_s \mathrm{PWF}(\mathrm{Ne},\ i,\ d) - \frac{r_v}{(1+d)^{\mathrm{Ne}}}, \tag{13}$$

$$\mathrm{LCT} = P_1 C_E \left(\frac{Q_c}{\mathrm{EER}} + \frac{Q_h}{\eta}\right) + P_2 C_{ins} x_{ins}, \tag{14}$$

$$\mathrm{AES} = \left(\frac{Q_c}{\mathrm{EER}} + \frac{Q_h}{\eta}\right)_{x_{ins}} - \left(\frac{Q_c}{\mathrm{EER}} + \frac{Q_h}{\eta}\right)_{x_{ins}=0}, \tag{15}$$

where PWF is the function of present worth factor; i and d are the fuel price inflation rate and market discount rate, respectively; Ne is the total time of economic analysis; D is the percent of down payment; m is the mortgage interest rate; m_s and r_v are the ratio of annual maintenance cost to initial investment and the ratio of resale price to initial investment, respectively; C_E and C_{ins} are the electrovalence and insulation costs, respectively; x_{ins} is the insulation thickness; N_L and N_{min} are the period of mortgage payments and the period of maturity, respectively; EER and η are the energy efficiency ratios of the cooling system and the heating system, respectively.

To simplify the optimization, and to highlight the boundary effects, taxation in the P_1–P_2 model was ignored in this study. Table 1 lists the values in the P_1–P_2 model (Liu et al., 2015).

Table 1 Values of parameters in the economic model (Liu et al., 2015)

Parameter	Value	Parameter	Value
d	0.05	D	1
i	0.01	m_s	0
Ne (a)	20	r_v	0
N_{min} (a)	NA	C_E (\$/(kW·h))	0.087
N_L (a)	NA	C_{ins} (\$/m^3)	50
m	NA	EER and η	2.3 and 1.9

NA represents that the parameter is not needed in the calculation when D=1

3 Case study

3.1 Description

The study is based on a residential building in Hangzhou, a city in the HSCW zone of China. The information about the building, wall configuration, and hygrothermal properties of the materials are listed in Section S3 of the ESM. The schedules of Q^{oc}_{iamb} and M^{oc}_{iamb} are listed in Fig. 3a. The total wall area is 113 m^2 with no windows. The total room volume is 196 m^3 and the air volume of HVAC system is 1 m^3/s. The meteorology data can be seen in Section S4 of the ESM (NOAA, 2001). The air pressure difference between the inside and outside of the building is set at 5 Pa. The HVAC system is a continuously operating multizone constant air volume (CAV) system air handling unit equipped with humidistats/de-humidistats. The HVAC system is ideal and assumed to have sufficient cooling/heating ability. The temperature/relative humidity set-points are 25 °C/0.7 in summer and 20 °C/0.4 in winter (MOHURD, 2012). The HVAC system remains in the cooling mode in summer and heating mode in winter. There is no other equipment in the building except the indoor heat and moisture emitted by the occupants.

3.2 Results

3.2.1 Effect of airtightness and internal heat source Q^{oc}_{iamb} on the optimum insulation thickness

The energy demands of a room are influenced by its airtightness and indoor heat and moisture sources. However, it is seen from Fig. 4 and Table 2 that the optimum insulation thicknesses are around 88.50–89.50 mm with different levels of indoor heat sources Q^{oc}_{iamb}. The optimum insulation thickness is obtained by the regression of the LCT curve. Compared to the baseline (A_{CH}=1 ACH, 100% Q^{oc}_{iamb}), the deviation of optimum insulation thickness is less than 1% when the internal heat sources changes from 75% Q^{oc}_{iamb} to 125% Q^{oc}_{iamb}, and the airtightness changes from 1 ACH to 2 ACH. Therefore, the effect of airtightness and internal heat sources on the optimum insulation thickness is slight. Recently, Landuyt et al. (2021) also showed that the optimum insulation thickness is hardly affected by user behaviour, which confirms our results.

When there is no insulation, the annual cooling load of a wall Q_c decreases and the annual heating load of a wall Q_h increases as the heat source Q^{oc}_{iamb} rises, and vice versa when the insulation is thickened (Fig. 4 and Section S5 of the ESM). Besides, for a level of airtightness, it can be seen from Fig. 4 that the value of A_{CH} is approximately proportional to the annual energy load of a wall, especially in the thin insulation cases. The optimum insulation thickness is smaller in cases with larger A_{CH}, and the values of AES are higher in those with larger A_{CH} (Fig. 4d). It should

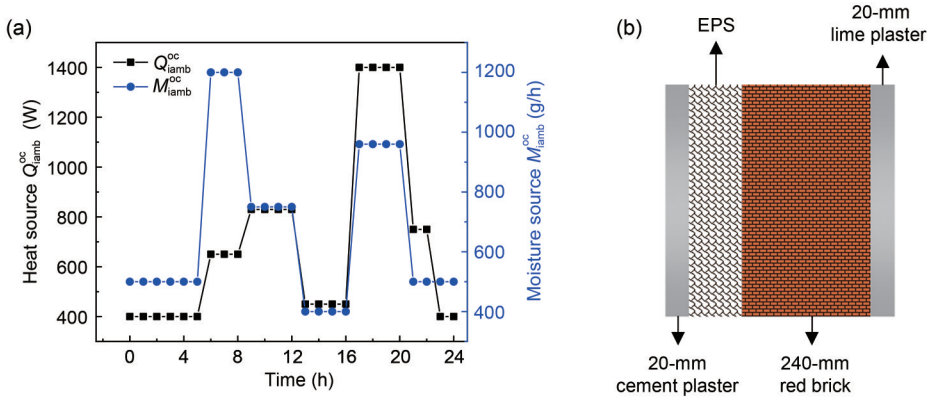

Fig. 3 Schematic diagrams of the case: (a) indoor heat and moisture sources (Tariku et al., 2011); (b) schematic diagram of the wall envelope. EPS represents the expanded polystyrene insulation

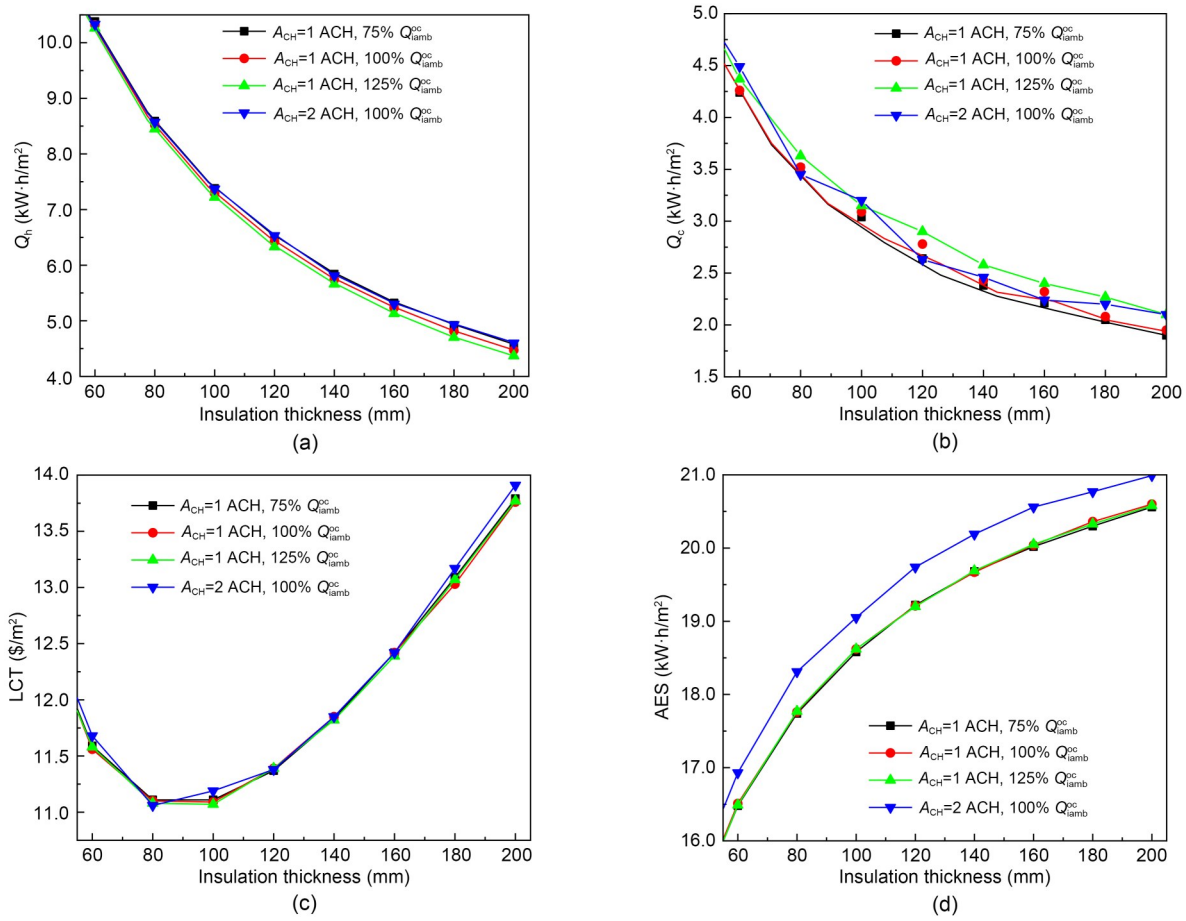

Fig. 4 Calculation results for different levels of airtightness and indoor heat sources of occupants: (a) annual energy loads of a wall in heating season; (b) annual energy loads of a wall in cooling season; (c) LCT; (d) AES

Table 2 Comparison of calculation results with different levels of indoor heat sources of occupants and airtightness in Fig. 3a

Model	Optimum insulation thickness $x_{op,ins}$ (mm)	Deviation of $x_{op,ins}$ (%)	LCT at $x_{op,ins}$ ($/m²)	Deviation LCT at $x_{op,ins}$ (%)	AES at $x_{op,ins}$ (kW·h/m²)	Deviation of AES at $x_{op,ins}$ (%)
A_{CH}=1 ACH, 75% Q^{oc}_{iamb}	89.50	0.34	11.07	0.18	18.17	−0.11
A_{CH}=1 ACH, 100% Q^{oc}_{iamb}	89.20		11.05		18.19	
A_{CH}=1 ACH, 125% Q^{oc}_{iamb}	89.00	−0.22	11.02	−0.27	18.20	0.05
A_{CH}=2 ACH, 100% Q^{oc}_{iamb}	88.50	−0.78	11.06	0.09	18.67	2.64

be noted that the energy load curves in Fig. 4a are not smooth in the summer, which may be due to the complex coupling behaviour of the high infiltration rate of WDR and water vapour.

3.2.2 Indicators of energy loads: energy loads of a wall Q_c/Q_h or the heat source of the HVAC system Q^{me}_{iamb}

Q_c and Q_h in Eq. (11) are the annual energy loads of a single wall, while Q^{me}_{iamb} in the IEM is the heat source caused by the HVAC system. Therefore, instead of the energy load of a single wall, Q^{me}_{iamb} can also be used in Eq. (14) of the economic analysis by $Q_c^* = -\frac{1}{A}\sum^{Nch} Q^{me}_{iamb}$ and $Q_h^* = \frac{1}{A}\sum^{Nhh} Q^{me}_{iamb}$. The sensible and latent heats are not involved in the Q_c^* and Q_h^*. It can be seen from the literature that some researchers have used the energy loads of a single wall to obtain the optimum insulation thickness (Liu et al., 2015; Dlimi et al., 2019), while others have used the whole energy demands of a building (D'Agostino et al., 2019; Geng

et al., 2021). However, a comparison of the suitability of these two indicators in the optimisation of insulation thickness is lacking.

Fig. 5 shows the LCT at A_{CH}=1 ACH and 100% Q^{oc}_{iamb} by using the heat source of the HVAC system Q^{me}_{iamb} as the indicator, as well as the result by using the energy load of a wall. Fig. 5 illustrates that although the LCT is different from each other, the optimum insulation thickness is nearly the same. Therefore, both indicators are valid in the optimization.

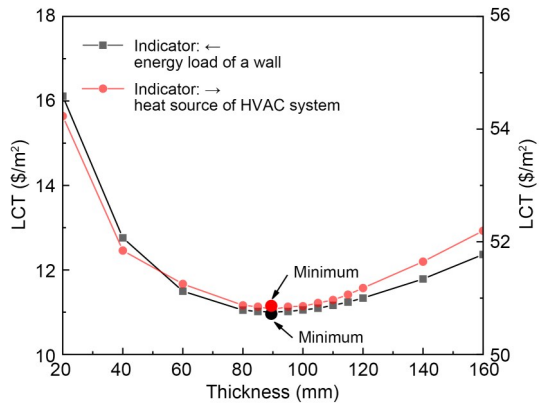

Fig. 5 Calculation results for A_{CH}=1 ACH and 100% Q^{oc}_{iamb} in Fig. 3a by using different indicators

3.3 Comparison with other transient optimization methods

There are several widely-used transient optimization methods for the insulation thickness of the exterior wall, such as the transient heat transfer model (TH) and the coupled heat and moisture transfer model (CHM).

The TH only takes account of the heat transfer process of a single wall by calculating the heat transfer equations. The outdoor boundary conditions of the TH consist only of the convection flow and solar radiation, while the indoor boundary condition is the constant temperature (Dlimi et al., 2019; Wang et al., 2019; Geng et al., 2021). The CHM takes account of the heat and moisture transfer of a single wall (Liu et al., 2015). The outdoor boundary conditions further consist of the moisture convection and WDR, while the indoor boundary conditions (indoor temperature and relative humidity) are set as constant (Tunçbilek et al., 2022).

Fig. 6 shows the results of the TH and CHM. The results of CHM indicate the similar Q_c and slightly higher Q_h when compared with the results of CHM. Meanwhile, the LCT and AES curves obtained by the CHM can be higher than the ones obtained by the TH. However, it is clearly shown in Fig. 6a that the Q_c and Q_h calculated by the HAM-IEM are higher than the results of the two other methods as the insulation thickness increases. In Fig. 6b, it can be seen that the LCT and AES calculated by the HAM-IEM deviate from the results of two other methods.

Table 3 and Fig. 7 are the comparison of the optimum insulation thicknesses calculated by three methods. The three enlarged points in Fig. 7 refer to the LCTs with optimum insulation thicknesses by different methods. It can be seen from Fig. 7 and Table 3 that the optimum insulation thicknesses obtained from the TH and the CHM are overestimated by 2.13% and 3.59% compared with those from the HAM-IEM in this study; the annual energy loads on a single wall (Q_c+Q_h) are underestimated by 11.44% and 10.10%

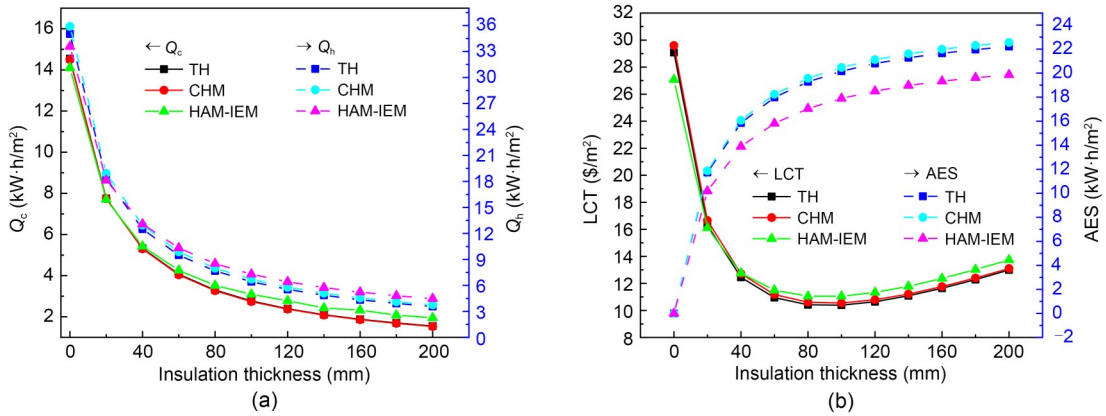

Fig. 6 Results of different transient optimization methods: (a) annual energy loads of a wall in the cooling and heating seasons; (b) LCT and AES

compared to those from using the HAM-IEM; the values of the minimum LCT at the optimum insulation thickness are underestimated by 6.24% and 4.71% compared to those from the HAM-IEM; the values of AES at optimum insulation thickness are overestimated by 8.91% and 10.83% compared to those from using the HAM-IEM. Liu et al. (2015) found that the optimum insulation thickness can be underestimated by 3.7%–7.8% if no moisture transfer in the wall is considered. However, in this study, the underestimation is only 1.3 mm (about 1.41%), which may be because of the different climate of the chosen cities.

Therefore, although all the cities in the literature (Liu et al., 2015) and this study are in the HSCW zone of China, the influence on the optimum insulation thickness caused by moisture transfer in the wall can still vary greatly. Moreover, Table 3 indicates that the indoor moisture buffering effect on the optimum insulation thickness is 3.59% ((92.40–89.20) mm/89.20 mm), while the effect caused by the moisture buffering in the wall is 1.41% ((92.40–91.10) mm/92.40 mm). The indoor moisture buffering effect is about 2.54 times larger than the moisture buffering effect in the exterior envelope. It is suggested that the indoor environment, such as the indoor temperature and relative humidity, should be considered when optimizing the insulation thickness of the exterior wall.

3.4 Discussion

The new HAM-IEM methodology proposed in this study can be applied to different combinations of occupants, airtightness, and configurations of the HVAC system. It can be used in different micro-climate buildings with different controlled systems. The proposed methodology can help with the personalised thermal design of a building within a specific city. The combination of HAM and IEM is easy to calculate numerically.

3.4.1 Average indoor temperature and relative humidity

The average indoor temperature and relative humidity are not constants in HAM-IEM (Fig. 8), and they can affect the calculation of energy consumption in Eq. (11).

It can be observed in Fig. 8a that the average indoor temperature under different insulation thicknesses is always higher than 298.15 K (constant) in the cooling season and lower than 293.15 K (constant) in the heating season. From Fig. 8b, the average indoor relative humidity under different insulation thicknesses is always lower than 0.7 (constant) in the cooling season and higher than 0.4 (constant) in the heating season. Besides, the variation becomes steady as the insulation gets thicker. Therefore, it is inappropriate to set the indoor temperature and relative humidity as constants in the optimization of insulation thickness.

3.4.2 Moisture buffering effect in the envelope

It is known that the moisture transfer in the wall can lead to an extra latent heat flow. The total heat capacity, as well as the buffering effect, is increased due to the moisture transfer (Liu et al., 2015). This latent heat flow is more pronounced during the heating season when the indoor temperature is lower (Table 4). Therefore, the energy consumption optimized by the CHM is higher than that optimized by the TH for all insulation thicknesses. In addition, the thinner the insulation, the greater the increase of energy consumption, which indicates that the moisture buffering effect is strong when the insulation thickness is small.

The LCT curve in Fig. 7 shows the same variation pattern as the energy consumption with the same

Table 3 Comparison of results with different transient optimization methods

Model	Optimum insulation thickness $x_{op,ins}$ (mm)	Deviation of $x_{op,ins}$ (%)	Annual energy load of a wall at $x_{op,ins}$ (kW·h/m^2)	Deviation of annual energy load of a wall at $x_{op,ins}$ (%)	LCT at $x_{op,ins}$ (\$/m^2)	Deviation of LCT at $x_{op,ins}$ (%)	AES at $x_{op,ins}$ (kW·h/m^2)	Deviation of AES at $x_{op,ins}$ (%)
TH	91.10	2.13	9.91	−11.44	10.36	−6.24	19.81	8.91
CHM	92.40	3.59	10.06	−10.10	10.53	−4.71	20.16	10.83
HAM-IEM in this study*	89.20		11.19		11.05		18.19	

* For cases with A_{CH}=1 ACH and 100% Q^{oc}_{iamb} in Fig. 3a

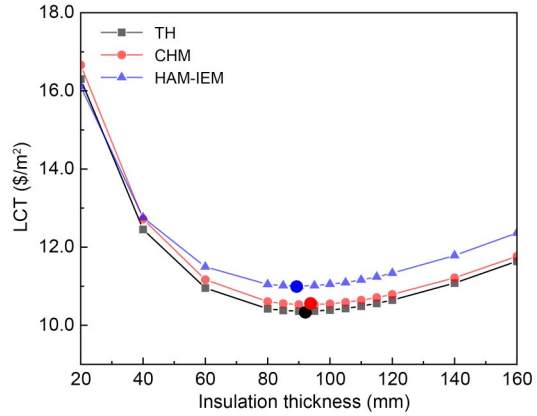

Fig. 7 Comparison of LCT and optimum insulation thickness with different transient optimization methods

investment cost. Therefore, the minimal value of the LCT curve is shifted to the side with larger insulation thickness. The optimum insulation thickness optimized by the CHM is shifted to the side of high insulation thickness and is higher than that optimized by the TH.

3.4.3 Indoor moisture buffering effect

In the HAM-IEM, the indoor humidity buffer effect is considered based on the CHM.

As can be seen from Table 4, the energy consumption is smaller than that calculated by the CHM when the insulation thickness is less than 20 mm (cooling season) and 40 mm (heating season). The reduction in energy consumption is due to these factors: (1) the temperatures at the interior surface of walls calculated by the CHM and the HAM-IEM are almost equal during the cooling season, while the temperatures at the interior surface of walls calculated by the HAM-IEM are higher during the heating season (Fig. 9); (2) the average indoor temperatures calculated by the HAM-IEM are higher or lower than those calculated by the CHM during the cooling or heating season (Fig. 8). Therefore, according to the definition of Q_c and Q_h in Eq. (11), the energy consumption of HAM-IEM is lower. By contrast, when the insulation is thicker, the energy consumption is greater than that calculated by the CHM, which also can be explained according to Figs. 8 and 9.

It is demonstrated that the energy consumption calculated by HAM-IEM does not increase for every thickness. Contrary to the moisture buffering effect in the envelope (Section 3.4.2), the thicker the insulation, the greater the increase of energy consumption as well as the indoor moisture buffering effect and the LCT curve. As a result, the minimal value of LCT curve is shifted to the side with the smaller insulation thickness, and that shift leads to a decrease in the optimal thickness. When the insulation is thicker, the relative percentage increase in energy consumption caused by the indoor moisture buffering effect is larger. Besides, when the insulation thickness is low, the indoor temperature and humidity cannot be considered as constant values, and the energy consumption will be lower than that obtained by the TH and CHM (Fig. 8).

The results in Fig. 8 and Table 4 also show that large deviations from the optimum insulation thickness come from small differences in the average indoor temperature, and that small differences in indoor temperature should not be ignored in the optimization. Thus, just like the heat transfer from the external atmosphere and the indoor heat source, the buffering effect of moisture can be viewed as a "two-sided" process. On the one hand, the moisture transfer from the outside atmosphere can increase the optimal insulation thickness due to the buffering effect. On the other

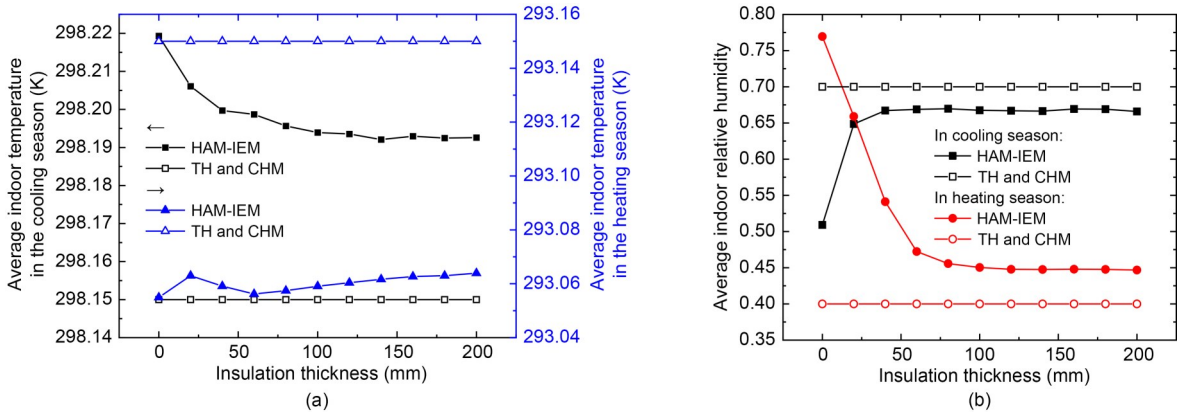

Fig. 8 Average indoor parameters in HAM-IEM: (a) indoor temperature; (b) indoor relative humidity

Table 4 Comparison of Q_c and Q_h in different cases and optimization methods*

x_{ins} (mm)	TH		CHM		HAM-IEM in this study	
	Q_c (kW·h/m^2)	Q_h (kW·h/m^2)	Q_c (kW·h/m^2)	Q_h (kW·h/m^2)	Q_c (kW·h/m^2)	Q_h (kW·h/m^2)
0	14.54	35.02	14.50	35.89	13.93	32.29
20	7.75	18.34	7.74	18.94	7.66	18.11
40	5.33	12.50	5.30	12.96	5.43	12.91
60	4.07	9.50	4.04	9.87	4.24	10.24
80	3.30	7.67	3.27	7.99	3.54	8.48
100	2.77	6.43	2.74	6.71	3.05	7.27
120	2.39	5.54	2.37	5.79	2.70	6.39
140	2.10	4.86	2.08	5.10	2.43	5.73
160	1.88	4.33	1.86	4.55	2.24	5.21
180	1.70	3.91	1.68	4.11	2.08	4.79
200	1.55	3.56	1.53	3.75	1.92	4.45

* The cases consist of different insulation thicknesses x_{ins}, with A_{CH}=1 ACH and 100% Q^{oc}_{iamb} in Fig. 3a. The values of green/orange color in the table represent the results of coupled numerical model, which are lower/higher than the results of CHM, respectively. References to color refer to the online version of this table

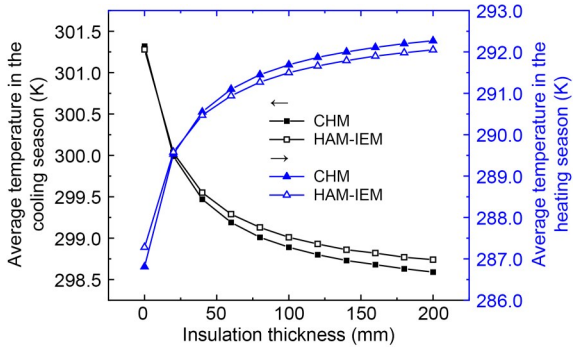

Fig. 9 Average temperature on the interior surface of the wall in the cooling and heating seasons

hand, the moisture transfer from the indoor atmosphere can have an adverse buffering effect on the optimum insulation thickness. The two buffering effects are in opposite directions. Therefore, as the thickness of insulation increases, it is more difficult for moisture from the indoor atmosphere to escape, requiring more energy load with the larger overall heat capacity.

The results indicate that the outward movement of the indoor heat and moisture can be hindered as the insulation layer is over-thickened, which can worsen the indoor environment and reduce thermal comfort (Olivieri et al., 2017; D'Agostino et al., 2019). It is suggested that HAM-IEM should be used to further investigate the optimum insulation thickness in various climate and building cases. Furthermore, it should be noted that since the moisture buffering effects of the indoor environment and the wall are opposite, the role of the moisture buffering effect in the envelope should not be over-emphasized in the optimization of insulation thickness (Fang et al., 2022).

Due to the counteraction of the moisture buffering effects that take place in the exterior wall and the indoor environment, excessive consideration of the insulation thickness can result from neglecting the indoor heat sources as well as the indoor moisture sources. Meanwhile, the study also suggests that the effect of moisture transfer in the optimization of insulation thickness is smaller than that has been previously thought. It should be noted that the effect of the moisture buffering effect in the envelope on the optimum insulation thickness (1.41%) is much lower than that in the previous study (3.7%–7.8%) (Liu et al., 2015), which indicates a different intensity of buffering occurs in the same climate zone. This should be further studied.

4 Conclusions

In this study, with consideration of the indoor moisture buffering effect, a new methodology, the HAM-IEM, is proposed to obtain the optimum insulation thickness of exterior walls in the HSCW zone in China. The airtightness, HVAC systems, and activities of the occupants were considered for the time-dependent indoor environment to represent reality. Some conclusions can be drawn from this study:

(1) The optimum insulation thickness obtained by TH or CHM may be overestimated by 2.13%–

3.59%; the annual energy loads on a single wall (Q_c+Q_h) may be underestimated by 11.44% and 10.10%; the minimum values of LCT at the optimum insulation thickness may be underestimated by 6.24% and 4.71%; the values of AES at the optimum insulation thickness may be overestimated by 8.91% and 10.83%.

(2) The two moisture buffering effects, the moisture buffering effect in the envelope, and the indoor moisture buffering effect, have the opposite effect on the optimum insulation thickness. The indoor moisture buffering effect is about 2.54 times greater than the moisture buffering effect in the envelope.

(3) The airtightness and indoor heat sources have a slight influence on the optimum insulation thickness, while the AES is higher for a larger A_{CH}.

(4) Two indicators of energy loads (the energy loads of a wall Q_c/Q_h and the heat source of the HVAC system) behave similarly in the optimization of insulation thickness.

In the future, the new methodology can be optimized for different climate zones and personalized indoor environments (Meng et al., 2015). As the personalized energy management system becomes popular, the users' behaviour and thermal comfort indices should be taken into consideration more carefully. As a result, the variance of indoor temperature and relative humidity becomes an unsteady process (Elmaz et al., 2021), and the optimum insulation thickness may be different from what has hitherto been believed.

Acknowledgments

This work is supported by the National Natural Science Foundation of China (Nos. 51978623 and 52076189).

Author contributions

Yan-hao FENG: investigation, conceptualization, data curation, methodology, software, validation, and writing–original draft. Zi-tao YU: project administration, supervision, and writing–review & editing. Jiang LU: project administration, supervision, and writing–review & editing. Xu XU: supervision.

Conflict of interest

Yan-hao FENG, Zi-tao YU, Jiang LU, and Xu XU declare that they have no conflict of interest.

References

Ali Kallioğlu M, Sharma A, Chinnasamy V, et al., 2021. Optimum insulation thickness assessment of different insulation materials for mid-latitude steppe and desert climate (BSH) region of India. *Materials Today: Proceedings*, 44:4421-4424. https://doi.org/10.1016/j.matpr.2020.10.590

ASHRAE (American Society of Heating, Refrigerating and Air Conditioning Engineers), 2016. Criteria for Moisture Control Design Analysis in Buildings, ASHRAE Standard 160:2016. ASHRAE, Atlanta, USA.

BSI (British Standards Institution) , 2012. Hygrothermal Performance of Building Components and Building Elements. Internal Surface Temperature to Avoid Critical Surface Humidity and Interstitial Condensation. Calculation Methods, BS EN ISO 13788:2012. BSI Standards Limited, London, UK.

Chbani Idrissi Y, Belarbi R, Ferroukhi MY, et al., 2022. Development of a numerical approach to assess the effect of coupled heat and moisture transfer on energy consumption of residential buildings in Moroccan context. *Journal of Building Physics*, 45(6):774-808. https://doi.org/10.1177/17442591211056068

Chen S, Zhang GM, Xia XB, et al., 2020. A review of internal and external influencing factors on energy efficiency design of buildings. *Energy and Buildings*, 216:109944. https://doi.org/10.1016/j.enbuild.2020.109944

Chung D, Wen J, Lo LJ, 2020. Development and verification of the open source platform, HAM-tools, for hygrothermal performance simulation of buildings using a stochastic approach. *Building Simulation*, 13(3):497-514. https://doi.org/10.1007/s12273-019-0594-5

D'Agostino D, De'Rossi F, Marigliano M, et al., 2019. Evaluation of the optimal thermal insulation thickness for an office building in different climates by means of the basic and modified "cost-optimal" methodology. *Journal of Building Engineering*, 24:100743. https://doi.org/10.1016/j.jobe.2019.100743

Dlimi M, Iken O, Agounoun R, et al., 2019. Energy performance and thickness optimization of hemp wool insulation and air cavity layers integrated in Moroccan building walls'. *Sustainable Production and Consumption*, 20:273-288. https://doi.org/10.1016/j.spc.2019.07.008

Duffie JA, Beckman WA, 1991. Solar Engineering of Thermal Processes. Wiley, Hoboken, USA, p.475-478.

Elmaz F, Eyckerman R, Casteels W, et al., 2021. CNN-LSTM architecture for predictive indoor temperature modeling. *Building and Environment*, 206:108327. https://doi.org/10.1016/j.buildenv.2021.108327

Fang JZ, Zhang HB, Ren P, et al., 2022. Influence of climates and materials on the moisture buffering in office buildings: a comprehensive numerical study in China. *Environmental Science and Pollution Research*, 29(10):14158-14175. https://doi.org/10.1007/s11356-021-16684-3

Fang ZS, Li N, Li BZ, et al., 2014. The effect of building envelope insulation on cooling energy consumption in summer. *Energy and Buildings*, 77:197-205. https://doi.org/10.1016/j.enbuild.2014.03.030

Ferroukhi MY, Djedjig R, Belarbi R, et al., 2015. Effect of coupled heat, air and moisture transfers modeling in the wall on the hygrothermal behavior of buildings. *Energy*

Procedia, 78:2584-2589. https://doi.org/10.1016/j.egypro.2015.11.293

Geng YC, Han X, Zhang H, et al., 2021. Optimization and cost analysis of thickness of vacuum insulation panel for structural insulating panel buildings in cold climates. *Journal of Building Engineering*, 33:101853. https://doi.org/10.1016/j.jobe.2020.101853

Hagentoft CE, Kalagasidis AS, Adl-Zarrabi B, et al., 2004. Assessment method of numerical prediction models for combined heat, air and moisture transfer in building components: benchmarks for one-dimensional cases. *Journal of Thermal Envelope and Building Science*, 27(4):327-352. https://doi.org/10.1177/1097196304042436

Hens HLSC, 2015. Combined heat, air, moisture modelling: a look back, how, of help? *Building and Environment*, 91: 138-151. https://doi.org/10.1016/j.buildenv.2015.03.009

Kaynakli O, 2012. A review of the economical and optimum thermal insulation thickness for building applications. *Renewable and Sustainable Energy Reviews*, 16(1):415-425. https://doi.org/10.1016/j.rser.2011.08.006

Landuyt L, de Turck S, Laverge J, et al., 2021. Balancing environmental impact, energy use and thermal comfort: optimizing insulation levels for the mobble with standard HVAC and personal comfort systems. *Building and Environment*, 206:108307. https://doi.org/10.1016/j.buildenv.2021.108307

Li BZ, Du CQ, Yao RM, et al., 2018. Indoor thermal environments in Chinese residential buildings responding to the diversity of climates. *Applied Thermal Engineering*, 129: 693-708. https://doi.org/10.1016/j.applthermaleng.2017.10.072

Liu XW, Chen YM, Ge H, et al., 2015. Determination of optimum insulation thickness for building walls with moisture transfer in hot summer and cold winter zone of China. *Energy and Buildings*, 109:361-368. https://doi.org/10.1016/j.enbuild.2015.10.021

Martínez-Mariño S, Eguía-Oller P, Granada-Álvarez E, et al., 2021. Simulation and validation of indoor temperatures and relative humidity in multi-zone buildings under occupancy conditions using multi-objective calibration. *Building and Environment*, 200:107973. https://doi.org/10.1016/j.buildenv.2021.107973

Meng QL, Yan XY, Ren QC, 2015. Global optimal control of variable air volume air-conditioning system with iterative learning: an experimental case study. *Journal of Zhejiang University-SCIENCE A (Applied Physics & Engineering)*, 16(4):302-315. https://doi.org/10.1631/jzus.A1400137

MOHURD (Ministry of Housing and Urban-Rural Development of the People's Republic of China), 2010. Design Standard for Energy Efficiency of Residential Buildings in Hot Summer and Cold Winter Zone, JGJ 134-2010. National Standards of the People's Republic of China (in Chinese).

MOHURD (Ministry of Housing and Urban-Rural Development of the People's Republic of China), 2012. Design Code for Heating Ventilation and Air Conditioning of Civil Buildings, GB 50736-2012. National Standards of the People's Republic of China (in Chinese).

Moon HJ, Ryu SH, Kim JT, 2014. The effect of moisture transportation on energy efficiency and IAQ in residential buildings. *Energy and Buildings*, 75:439-446. https://doi.org/10.1016/j.enbuild.2014.02.039

NOAA (National Oceanic and Atmospheric Administration), 2001. Global Hourly-Integrated Surface Database (ISD). https://www.ncei.noaa.gov/products/land-based-station/integrated-surface-database

Olivieri F, Grifoni RC, Redondas D, et al., 2017. An experimental method to quantitatively analyse the effect of thermal insulation thickness on the summer performance of a vertical green wall. *Energy and Buildings*, 150:132-148. https://doi.org/10.1016/j.enbuild.2017.05.068

Qin MH, Yang J, 2016. Evaluation of different thermal models in energyplus for calculating moisture effects on building energy consumption in different climate conditions. *Building Simulation*, 9(1):15-25. https://doi.org/10.1007/s12273-015-0263-2

Qin MH, Belarbi R, Aït-Mokhtar A, et al., 2009. Simulation of coupled heat and moisture transfer in air-conditioned buildings. *Automation in Construction*, 18(5):624-631. https://doi.org/10.1016/j.autcon.2008.12.006

Rode C, Peuhkuri R, Woloszyn M, 2006. Simulation tests in whole building heat and moisture transfer. Proceedings of the 3rd International Building Physics Conference, p.527-534.

Tariku F, Kumaran K, Fazio P, 2010. Integrated analysis of whole building heat, air and moisture transfer. *International Journal of Heat and Mass Transfer*, 53(15-16):3111-3120. https://doi.org/10.1016/j.ijheatmasstransfer.2010.03.016

Tariku F, Kumaran K, Fazio P, 2011. Determination of indoor humidity profile using a whole-building hygrothermal model. *Building Simulation*, 4(1):61-78. https://doi.org/10.1007/s12273-011-0031-x

Trindade AD, Coelho GBA, Henriques FMA, 2021. Influence of the climatic conditions on the hygrothermal performance of autoclaved aerated concrete masonry walls. *Journal of Building Engineering*, 33:101578. https://doi.org/10.1016/j.jobe.2020.101578

Tunçbilek E, Komerska A, Arıcı M, 2022. Optimisation of wall insulation thickness using energy management strategies: intermittent versus continuous operation schedule. *Sustainable Energy Technologies and Assessments*, 49: 101778. https://doi.org/10.1016/j.seta.2021.101778

Wang SH, Kang YM, Yang ZL, et al., 2019. Numerical study on dynamic thermal characteristics and optimum configuration of internal walls for intermittently heated rooms with different heating durations. *Applied Thermal Engineering*, 155:437-448. https://doi.org/10.1016/j.applthermaleng.2019.04.005

Wang YY, Ma C, Liu YF, et al., 2018. A model for the effective thermal conductivity of moist porous building materials based on fractal theory. *International Journal of Heat*

and Mass Transfer, 125:387-399. https://doi.org/10.1016/j.ijheatmasstransfer.2018.04.063

Woloszyn M, Kalamees T, Olivier Abadie M, et al., 2009. The effect of combining a relative-humidity-sensitive ventilation system with the moisture-buffering capacity of materials on indoor climate and energy efficiency of buildings. *Building and Environment*, 44(3):515-524. https://doi.org/10.1016/j.buildenv.2008.04.017

Woods J, Winkler J, 2016. Field measurement of moisture-buffering model inputs for residential buildings. *Energy and Buildings*, 117:91-98. https://doi.org/10.1016/j.enbuild.2016.02.008

Xu CC, Li SH, Zou KK, 2019. Study of heat and moisture transfer in internal and external wall insulation configurations. *Journal of Building Engineering*, 24:100724. https://doi.org/10.1016/j.jobe.2019.02.016

Zhang MJ, Qin MH, Chen Z, 2017. Moisture buffer effect and its impact on indoor environment. *Procedia Engineering*, 205:1123-1129. https://doi.org/10.1016/j.proeng.2017.10.417

Zhang YM, Jie PF, Liu CH, et al., 2022. Optimizing environmental insulation thickness of buildings with CHP-based district heating system based on amount of energy and energy grade. *Frontiers in Energy*, 16:613-628. https://doi.org/10.1007/s11708-020-0700-5

Zhou XH, Carmeliet J, Sulzer M, et al., 2020. Energy-efficient mitigation measures for improving indoor thermal comfort during heat waves. *Applied Energy*, 278:115620. https://doi.org/10.1016/j.apenergy.2020.115620

Electronic supplementary materials

Sections S1–S5